Longitudinal study of tumor-associated macrophages during tumor expansion using MRI

Yen-Yu I. Shih[a,b], **Yi-Hua Hsu**[a], **Timothy Q. Duong**[b], **Sui-Shan Lin**[a], **Kai-Ping N. Chow**[c,*], and **Chen Chang**[a,**]

[a]Functional and Micro-Magnetic Resonance Imaging Center, Institute of Biomedical Sciences, Academia Sinica, Taipei, Taiwan

[b]Research Imaging Institute, University of Texas Health Science Center at San Antonio, San Antonio, TX, USA

[c] Department of Microbiology and Immunology, Chang-Gung University, Taiwan

Abstract

MRI is being used increasingly for the noninvasive longitudinal monitoring of cellular processes in various pathophysiological conditions. Macrophages are the main stromal cells in neoplasms and have been suggested to be the major cell type ingesting superparamagnetic iron oxide (SPIO) nanoparticles. However, no MRI study has described longitudinally the presence of tumor-associated macrophages (TAMs) during tumorigenesis with histological confirmation. To address this, we injected SPIO nanoparticles into the circulation of tumor-bearing mice and used MRI and post-mortem histology to monitor TAMs at different time points. The MRI results demonstrated that TAMs, as hypointense signals, appeared continually with the expansion of the tumor. The histological findings also revealed that SPIO-labeled TAMs tended to deposit closer to the vessel lumen with time prior to rapid tumor growth. The present study demonstrates the potential of using MRI to assess longitudinally TAM accumulation during tumorigenesis, and provides the first *in vivo* insight into the topographical arrangement of TAMs in relation to the progression of tumors. *In vivo* monitoring of the presence of TAMs could be useful for the development of tumor treatments that target TAM functions.

Keywords

tumor-associated macrophages; superparamagnetic iron oxide; tumor microenvironment

INTRODUCTION

MRI enables comprehensive assessment of the tumor micro-environment, including the vascular supply, metabolic changes, hypoxia and acidity (1,2). Recent advances using an MRI contrast agent – superparamagnetic iron oxide (SPIO) nanoparticles – have further improved our understanding of the intrinsic cellular mechanisms and tumorigenesis (3–7). Tumor-associated macrophages (TAMs), one of the major leukocytic cell types residing in tumor tissues, are observed concomitantly with the onset of tumor growth, and have been implicated in tumor promotion (8–14). There is accumulating evidence that high levels of

*Correspondence to: K.-P. N. Chow, Department of Microbiology and Immunology, Chang-Gung University, Kwei-Shan, Tao-Yuan 333, Taiwan. kpc@mail.cgu.edu.tw. ** Correspondence to: C. Chang, Institute of Biomedical Sciences, Academia Sinica, Taipei 115, Taiwan. bmcchen@ibms.sinica.edu.tw.

TAMs are often associated with a poor response to tumor treatments (14,15), whereas depletion of TAMs prevents tumors from progressing further (16,17). The targeting of TAM functions has been shown to be an effective anti-angiogenic therapeutic approach (9,10,16,17). Thus, the ability to noninvasively image and longitudinally monitor TAM distribution would be immensely beneficial.

Cells can be tracked using MRI by *ex vivo* labeling with SPIO nanoparticles and detected *in vivo* as hypointensity on T_2- or T_2*-weighted images (3,4). Although this method has been used to delineate the fate of macrophages in different pathophysiological experimental conditions (18–20), it is difficult to apply in clinical practice. As demonstrated by Moore *et al.* (21) and Williams *et al.* (22), the SPIO labeling efficiency is higher in macrophages than in other cell types. Alternatively, macrophages can be labeled *in vivo* or *in situ*. Clear co-localization of macrophages and SPIO nanoparticles has been shown to occur several days after a single systemic injection (23–27), indicating that the macrophages or monocytes take up SPIO nanoparticles with subsequent infiltration to their destination. These results demonstrate the potential of the systemic administration of SPIO nanoparticles for the tracking of macrophages *in vivo*.

The purpose of this study was to determine whether MRI could be used to monitor longitudinally the presence of TAMs during tumorigenesis. To this end, we used a single systemic administration of SPIO nanoparticles to track TAMs in a transplantable tumor model that is highly predictable, reproducible and can be easily infiltrated with macrophages (28,29). Post-mortem histology was also employed to serially identify the occurrence of SPIO-labeled TAMs. Our findings demonstrate the potential of using MRI to track TAMs, and provide the *in vivo* evidence that the expansion of new tumor mass is tightly associated with the presence of TAMs. The results of this study could facilitate the longitudinal assessment of potential TAM-targeting drugs for cancer therapy *in vivo*.

MATERIALS AND METHODS

Subjects and tumor model

Twenty-three male BALB/c mice (National Laboratory Animal Center, Taipei, Taiwan) were used for MRI experiments and histology. A transplantable tumor model mimic viral oncogene-mediated carcinogenesis with stable TAM infiltration was established by tumorigenesis of the Epstein–Barr virus-encoded oncogene latent membrane protein 1 (LMP1), as described previously (28,29). To facilitate *in vivo* tumor formation, LMP1-transformed BALB/c-3T3 cells were injected subcutaneously into five severe combined immunodeficiency (SCID) mice (4–5 weeks of age) for the development of solid tumor as passage 1. Small fragments (~9 mm^3) of passage 1 tumors that were known to be more immune resistant were taken from a SCID mouse showing most apparent tumor kinetics (29) and transplanted into the left flanks of five normal BALB/c mice (6–8 weeks of age) as passage 2. Afterwards, the tumor model was maintained among BALB/c mice by fragment transplantation (*n*=5 for each passage). This model has been shown to exhibit stable LMP1 expression, macrophage infiltration and tumor kinetics for at least 30 *in vivo* passages (29). In this study, the eighth to tenth passages were used. The day on which solid tumor fragments from tumor-bearing BALB/c mice were implanted subcutaneously into normal BALB/c mice was designated as day 0. All experimental procedures were approved by the Institute of Animal Care and Utilization Committee at Academia Sinica, Taipei, Taiwan.

MRI experiments and data processing

All MRI experiments were performed using a 7-T scanner (PharmaScan 70/16, Bruker Biospin GmbH, Ettlingen, Germany) with an actively shielded gradient of 300 mT/m in 80

μs. A volume coil with an internal diameter of 38 mm was used for both radiofrequency excitation and signal detection. On the day of the experiment, each animal was initially anesthetized with 5% isoflurane in O_2 at a flow rate of 5 L/min, and anesthesia was maintained with 1% isoflurane in O_2 at a flow rate of 1 L/min throughout the experiment. The anesthetized mice were immobilized using a customized body holder inside the magnet. The body temperature was kept at 37°C using a circulating warm-water blanket. The respiratory rate was monitored and maintained at 20–30 breaths/min by altering the isoflurane level.

In order to demonstrate the fate of SPIO particles in tumors *in vivo*, a group of tumor-bearing mice ($n = 6$) on day 5 were first scanned to obtain control T_2-weighted images using a rapid acquisition with relaxation enhancement (RARE) sequence with the following parameters: TR/TE = 5000/60 ms; RARE factor, 8; number of excitations, 4. T_2^*-weighted images were then acquired using a two-dimensional fast low-angle shot (FLASH) sequence with the following parameters: TR/TE = 600/13 ms; number of excitations, 2; flip angle, 15°. After imaging, dextran-coated SPIO particles (Feridex IV, Berlex Laboratories, Wayne, NJ, USA) were administered at a dose of 30 mg Fe/kg via the ophthalmic vein. T_2-and T_2^*-weighted images were then acquired immediately after SPIO particle injection and on days 7, 9, 11, 14 and 21. All images were obtained in the transverse direction with a field of view of 3 cm, slice thickness of 1 mm and a 256×128 matrix zero filled to 256×256. Images were reconstructed using ParaVision (Bruker Medical GmbH, Ettlingen, Germany), and the signal intensity was measured with MRVision (MRVision Co., Winchester, MA, USA). The tumor volume was calculated from the three-dimensional reconstruction of MR images using Amira (Visage Imaging GmbH, Berlin, Germany). The tumor volumetric doubling time was defined as described previously (28).

Histological examinations

To determine the correlation between MRI signal changes and histological data, a group of nine tumor-bearing mice was prepared, scanned as described previously and sacrificed after MRI experiments at representative time points on days 5,7 and 14 ($n = 3$ for each time point). Another group of six tumor-bearing mice without SPIO particle injection was scanned as controls and sacrificed after MRI experiments on days 5, 7 and 14 ($n = 2$ for each time point). The mice were perfused transcardially with 4% paraformaldehyde (Sigma, St Louis, MO, USA) in phosphate-buffered saline (PBS, pH 7.4). The tumors were removed, kept in the same fixative overnight at 4 °C, paraffinized and sectioned at 5 μm. The tumor sections were deparaffinized through xylene and graded alcohols prior to staining. Hematoxylin and eosin staining was used to reveal the tumor morphology on the images, and Prussian blue (PB) staining was performed to reveal the distribution of SPIO nanoparticles in tumors and thereby to allow the cause of MRI signal changes to be determined. Hematoxylin and eosin staining was performed on sections adjacent to PB staining. Immunostaining was used to identify cells containing SPIO particles and to assess tumor angiogenesis. An antibody against CD68 (MCA1957, AbD Serotec, Kidlington, Oxford UK) was used to identify monocytes/macrophages, and antibodies against CD31 (sc-1506, Santa Cruz Biotechnology, Inc., Santa Cruz, CA, USA) and α-smooth muscle actin (SMA) (ab5694, Abcam, Cambridge, MA, USA) were used to examine the vascular network. Briefly, deparaffinized sections were immersed in 10 m$_M$ citrate buffer (pH 6.0) at 98 °C for 30 min to retrieve the antigen. After washing with PBS containing 0.3% Triton X-100, sections were treated with 0.2% H_2O_2 in PBS to inhibit endogenous peroxidase. Nonspecific binding was blocked by the incubation of sections for 1 h in 3% normal serum plus 2% bovine serum albumin in PBS containing 0.3% Triton X-100. Sections were then incubated sequentially with the primary antibodies overnight at room temperature, with a biotinylated secondary antibody for 1 h and with an avidin–biotin–horseradish peroxidase

complex for 1 h. The antigen complex was then deposited with a diamino-benzidine solution (4 mg/mL in PBS) in the presence of 0.01% H_2O_2, and PB staining was performed thereafter. The double-staining slides were reviewed and counted under a microscope (BX51, Olympus, Tokyo, Japan) by two histologists (YHH and KPC) blind to the experimental groups. The SPIO labeling percentages in the total TAM population were calculated by dividing the number of PB-/CD68-positive cells by the number of CD68-positive cells. Nine mice (three slices per mouse) were analyzed for the quantification of PB- and CD68-positive cells.

Extraction of circulating leukocytes and bone marrow cells

To examine the existence of SPIO-labeled cells outside the tumor, two tumor-bearing mice were prepared. After the administration of SPIO particles on day 5, the extraction of circulating leukocytes and bone marrow cells was performed on days 6 and 14. The extracted cells were then cytospun to slides at a concentration of 1×10^5 cells/per slide. After air drying, the slides were immersed in 4% paraformaldehyde in PBS for fixation. After 10 min of fixation, the slides were washed in PBS and underwent double staining for CD68 and PB.

RESULTS

Progressive tumor growth is related to the appearance of MRI hypointensities

Figure 1 shows that the implanted tumors ($n = 6$) exhibited typical exponential growth (28,29). In general, the tumor growth was relatively slow at days 5–14 in comparison with the rapid growth at days 14–21. The initial growth of tumor on day 5 was minimal with a budding of new tumor mass. The location of budding varied among different animals, but usually occurred only on one side of the implanted fragment. The growth curve was calculated from mice with SPIO nanoparticle injection. The tumor volumetric doubling time in SPIO-injected mice was 4.53 ±0.97 days, whereas our previous study showed the doubling time in mice without SPIO nanoparticle injection was 4.19 ±0.73 days (28). No significant difference was found between the two groups (p > 0.05, t-test). In Fig. 2 (left panel), budding of the new tumor mass occurred on the left side of the fragment (dotted circles). The tumor continued to expand leftward, downward and then upward relative to the area in which budding first occurred.

To assess the presence of TAMs during tumor growth, SPIO nanoparticles were injected intravenously on day 5 to label TAMs *in vivo*. Figure 2 illustrates that the progressive development of the tumor mass was accompanied by the appearance of hypointensities that putatively represent SPIO-labeled TAMs. Interestingly, these hypointensities appeared in a stepwise manner in the tumor tissue. In the two representative cases, the hypointensity (red arrow, labeled 5 in the figure) appeared in the budding tumor area on both T_2*- and T_2-weighted images after the injection of SPIO nanoparticles on day 5 (Fig. 2). The hypointensity was more apparent in T_2*- than in T_2-weighted images, showing the high sensitivity of T_2*-weighted images to SPIO particles within tumor tissue. On day 7, the expansion of a new tumor mass (white arrow, labeled 7 in the figure) was observed close to the hypointensity found on day 5, together with newly detected hypointensities (red arrows, labeled 7 and 7' in the figure). The development of tumor mass near new hypointensities on subsequent days (days 9–14) continued in the same pattern as described above. Thus, there appeared to be a specific topographical relationship between the hypointensities and the newly formed tumor masses, beginning with a hypointensity at the side of the tumor that generated a new tumor mass, which itself served as the anchor for the formation of new tumor masses.

MRI hypointensity induced by SPIO-labeled TAMs

To verify whether MRI hypointensities in tumor tissue corresponded to SPIO particles, another set of tumors ($n = 9$) showing hypointensity (red arrows in Fig. 3a) after SPIO injection was collected at different time points. The tumors were sectioned and co-stained with PB (Fig. 3b) to depict iron particles (i.e. SPIO) and immunostained against CD68 (30) to identify macrophages. The PB deposits in the sections (Fig. 3c) corresponded to the distribution of hypointensities on the images. The enlarged views of PB-stained sections in Fig. 3d demonstrate that blue iron particles were consistently confined within CD68-positive cells on different days, showing that MR hypointensities were probably induced by SPIO-labeled TAMs. To depict the percentage of SPIO-labeled TAMs in the whole TAM population, the PB-/ CD68-positive and CD68-positive cells on the co-stained sections were counted directly under the microscope. The percentages of SPIO-labeled TAMs were 6.4 ±0.2%, 3.8 ±0.7% and 0.9 ±0.1% (mean ± standard deviation, $n = 3$ for each time point) on days 5, 7 and 14, respectively.

Another group of tumor-bearing mice without SPIO particle injection was imaged as a control group to verify the contribution of other potential sources to MR hypointensities ($n = 6$). Mild signal loss was observed in the new tumor mass on days 5 and 14 (Fig. 4a), but no clear iron deposit was found in the corresponding PB-stained sections (Fig. 4c, enlarged views from Fig. 4b). Adjacent hematoxylin and eosin-stained sections indicated that this signal loss was probably induced by hemorrhage (Fig. 4d). Compared with days 5 and 14, PB staining indicated the presence of iron-labeled cells in the hypointense area on day 7 (Fig. 4b, c), where hematoxylin and eosin-stained sections confirmed extensive hemorrhage (Fig. 4d). Although hemorrhage may also contribute to MR signal loss, the images from controls exhibited a different signal distribution pattern and less signal loss compared with the SPIO-injected group.

The presence of extratumoral SPIO-/CD68-positive cells

To determine whether additional blood and bone marrow-derived macrophages were labeled *in vivo*, blood and bone marrow cells were collected from another set of mice ($n = 2$) on days 6 and 14 and co-stained with PB and immunostained against CD68. PB-/CD68-positive cells were found on both days 6 and 14 (Fig. 5). On day 6, the percentages of PB-/CD68-positive cells over the total CD68-positive cells in the blood and bone marrow were 0.8 ±0.3% and 0.4 ±0.1%, respectively. On day 14, the percentage was 0.1 ±0.0% for both blood and bone marrow.

TAM distribution

To verify the locations of SPIO-labeled TAMs, PB staining and immunostaining against CD31 (31) (a marker of both mature and immature vessels) were performed separately on adjacent sections at each time point (Fig. 6a). On day 5, the iron-labeled cells (red arrows in the figure) were mainly distributed in the new tumor mass with relatively few and sparse vessels (asterisks in the figure). On day 14, the iron-labeled cells were found in the proximity of CD31-positive vessels (Fig. 6b, c). To rule out the possibility that SPIO particles were internalized by epithelial cells and/or pericytes/myofibroblasts in the vessel wall, co-staining of PB and CD31 or SMA (32) (a marker of pericytes/myofibroblasts) was performed. As shown in Fig. 6d, e, PB-positive cells were not CD31- or SMA-positive.

DISCUSSION

The present study demonstrates that MRI with the systemic administration of SPIO nanoparticles is able to assess longitudinally the presence of TAMs during tumorigenesis. TAMs are incorporated into the tumor expansion, with the appearance of TAM-related MR

hypointensity serving as an anchoring point for the subsequent addition of new tumor masses. Moreover, SPIO-labeled TAMs in developing tumor tissues appear closer to the vessels with time. These processes occur prior to rapid tumor growth (after day 14), indicating that TAMs may be associated with multiple steps of tumor angiogenesis at the initial stages.

Iron-laden TAMs and MR hypointensities

The use of the systemic injection of iron oxide particles to label macrophages has been investigated in various pathophysiological conditions, including ischemic stroke (27), multiple sclerosis (23), atherosclerosis (24), encephalomyelitis (26), neuroinflammation (20) and transplant rejection (25). It is generally agreed that hypointensities on subsequently acquired images indicate the presence of iron oxide particles, which are mainly internalized by macrophages as a result of phagocytic activity, with the magnitude of hypointensity being proportional to the iron content in the imaged tissue (24). A larger MR hypointense area has also been implicated to indicate a larger amount of iron-labeled macrophages in the corresponding section (25).

The hypointense areas on the images may also reflect local vasculature (33,34). Nevertheless, the MR signal from the vessels can be suppressed significantly by pure O_2 inhalation (33,34), making SPIO-labeled TAMs identifiable from vessels. In addition, hemorrhage in the tumor stroma can also lead to MR hypointensities (18). In this case, TAMs in hemorrhagic tumor tissue may become laden with iron as a result of the ingestion of by-products of red blood cell breakdown and/or the high local concentration of hemoglobin. Nevertheless, iron-labeled TAMs were also consistently observed in the tumor microenvironment without hemorrhage in SPIO-injected mice. Taken together, our findings suggest caution when interpreting MRI data during the hemorrhagic phase without another modality to verify the source of iron.

Sources of SPIO-labeled TAMs

SPIO particles have an intravascular half-life of a few minutes (35). Weissleder *et al.* (35) showed that 82% of the injected Feridex accumulates in the liver (half-life, 3 days) and 6% in the spleen (half-life, 4 days). It is unlikely that the particles alone in the bloodstream would continuously feed into the tumor several days after injection and label the stromal TAMs. We suspect that the MR hypointensities in the tumor microenvironment originate primarily from SPIO-labeled macrophages in blood and bone marrow. It has been shown that the internalized Feridex particles remain inside the cellular endosomes/lysosomes for at least 5 days (36). Vande Berg et al. (37) demonstrated that intravenously injected Feridex decreased the bulk T_2 value in human bone marrow for up to 3 weeks. More recently, Henning *et al.* (38) showed that rats preloaded with Feridex (intravenously), 7 days prior to stroke, exhibited iron-labeled bone marrow-derived macrophage infiltration in the ischemic cortex after 14 days. Our results from blood and bone marrow extraction also showed SPIO-labeled CD68-positive cells on days 6 and 14, demonstrating that SPIO-labeled TAMs (but not SPIO particles alone in the bloodstream) accumulated on days 7–14 can be derived from the bone marrow and recruited from the circulation. The ratio of PB-/CD68-positive cells decreased in the blood and bone marrow over time, which correlated well with that in the tumor. In addition, no PB-positive cells were seen on days 5 and 14 in the hypointense areas in the control group (without SPIO injection), but could be clearly identified in the SPIO injection group. This implies that TAMs can be labeled *in vivo* by a single bolus SPIO nanoparticle injection and continually recruited by tumor tissue.

In situ labeling of TAMs is also possible. It cannot be ruled out that SPIO nanoparticles injected on day 5 may extravasate from leaky vasculature at the tumor site and reside within

the tumor microenvironment for a certain period of time. In this case, the tumor microenvironment functions as an *in situ* storage of SPIO particles, which can be cleared by infiltrating macrophages (39) and also stained as PB-/CD68-positive TAMs. Although this may not be the major source of MRI hypointensity, these TAMs could still be recruited to form new MR hypointense spots. Consequently, TAMs can be labeled *in vivo* or *in situ*. Both views, however, do not alter the central conclusion that SPIO-labeled TAMs can be longitudinally detected by MRI during tumorigenesis, as confirmed by histology, and that the TAM-associated MR hypointense area serves as an anchor point for tumor expansion.

Tumorigenesis and TAMs

Highly vascularized networks supplying abundant oxygen and nutrients are indispensable to rapid tumor growth (40). Therefore, transformation of a tumor from a nonangiogenic phenotype to an angiogenic phenotype [i.e. the angiogenic switch (41,42)] is essential to achieve both tumor growth and the required vascularization. In this view, avascular areas of tumors are unfavorable for tumor development unless angiogenesis is 'switched on' (43). TAMs are known to induce endothelial cell migration and proliferation by releasing proangiogenic factors (12). It is therefore possible that the location of TAMs in the avascular regions of the early tumor (i.e. day 5) is related to the angiogenic switch and can produce new vascular networks for tumor growth (43). Consistent with this, our pilot study using dynamic contrast-enhanced MRI to investigate an identical tumor model showed that the vascular permeability started to increase on day 5 and then changed proportionally with the tumor volume over time (28).

Despite angiogenesis, the tumor vasculature is prone to collapse because of its disorganized and leaky nature (44). This results in hemorrhage in the primarily vascularized regions, as seen in our histology results on day 7. The hemorrhagic areas tend to become hypoxic to recruit more macrophages (45) to remove dead cells and release proangiogenic factors. As a consequence, the interstitial matrix of the tumor tissues undergoes remodeling and revascularization (45).

With the progression of tumor growth, TAMs reside in close apposition to the lumen of capillaries in the significantly enlarged tumor (i.e. day 14). TAMs at this stage are believed to differentiate into endothelial-like cells and become part of the tumor vasculature (46–48). Interestingly, the temporal evolution in the present study (i.e. days 5–14) was prior to the rapid growth phase. Although the underlying mechanisms warrant further investigation, we suspect that the observed behavior of TAMs may be part of the machinery promoting the angiogenic switch, and can be reliably detected by MRI.

CONCLUSION

The present study demonstrates the potential of MRI to monitor longitudinally the presence of TAMs in tumorigenesis with a single SPIO nanoparticle injection. The TAM-associated MR hypointense area serves as an anchor point for tumor expansion and SPIO-labeled TAMs gradually appear closer to vessels within 14 days. Our findings may benefit the future study of TAM behavior in tumors and the development of macrophage-targeted therapies. Future studies will employ fluorescent iron oxide particles to validate the source of iron in TAMs during tumorigenesis.

Acknowledgments

Abbreviations used

LMP1	Epstein–Barr virus-encoded oncogene latent membrane protein 1
PB	Prussian blue
PBS	phosphate-buffered saline
RARE	rapid acquisition with relaxation enhancement
SCID	severe combined immunodeficiency
SMA	α-smooth muscle actin
SPIO	superparamagnetic iron oxide
TAMs	tumor-associated macrophages.

REFERENCES

1. Gillies RJ, Raghunand N, Karczmar GS, Bhujwalla ZM. MRI of the tumor microenvironment. J. Magn. Reson. Imaging. 2002; 16(4):430–450. [PubMed: 12353258]

2. He Q, Xu RZ, Shkarin P, Pizzorno G, Lee-French CH, Rothman DL, Shungu DC, Shim H. Magnetic resonance spectroscopic imaging of tumor metabolic markers for cancer diagnosis, metabolic phenotyping, and characterization of tumor microenvironment. Dis. Markers. 2003; 19(2–3):69–94. [PubMed: 15096706]

3. Rogers WJ, Meyer CH, Kramer CM. Technology insight: in vivo cell tracking by use of MRI. Nat. Clin. Pract. Cardiovasc. Med. 2006; 3(10):554–562. [PubMed: 16990841]

4. Hoehn M, Wiedermann D, Justicia C, Ramos-Cabrer P, Kruttwig K, Farr T, Himmelreich U. Cell tracking using magnetic resonance imaging. J. Physiol. 2007; 584(Pt 1):25–30. [PubMed: 17690140]

5. Shapiro EM, Sharer K, Skrtic S, Koretsky AP. In vivo detection of single cells by MRI. Magn. Reson. Med. 2006; 55(2):242–249. [PubMed: 16416426]

6. Arbab AS, Pandit SD, Anderson SA, Yocum GT, Bur M, Frenkel V, Khuu HM, Read EJ, Frank JA. Magnetic resonance imaging and confocal microscopy studies of magnetically labeled endothelial progenitor cells trafficking to sites of tumor angiogenesis. Stem Cells. 2006; 24(3):671–678. [PubMed: 16179427]

7. Shapiro EM, Skrtic S, Sharer K, Hill JM, Dunbar CE, Koretsky AP. MRI detection of single particles for cellular imaging. Proc. Natl. Acad. Sci. USA. 2004; 101(30):10901–10906. [PubMed: 15256592]

8. Leek RD, Landers RJ, Harris AL, Lewis CE. Necrosis correlates with high vascular density and focal macrophage infiltration in invasive carcinoma of the breast. Br. J. Cancer. 1999; 79(5–6):991–995. [PubMed: 10070902]

9. Allavena P, Sica A, Solinas G, Porta C, Mantovani A. The inflammatory micro-environment in tumor progression: the role of tumor-associated macrophages. Crit. Rev. Oncol. Hematol. 2008; 66(1):1–9. [PubMed: 17913510]

10. Lewis C, Murdoch C. Macrophage responses to hypoxia: implications for tumor progression and anti-cancer therapies. Am. J. Pathol. 2005; 167(3):627–635. [PubMed: 16127144]

11. Biswas SK, Sica A, Lewis CE. Plasticity of macrophage function during tumor progression: regulation by distinct molecular mechanisms. J. Immunol. 2008; 180(4):2011–2017. [PubMed: 18250403]

12. Dirkx AE, Oude Egbrink MG, Wagstaff J, Griffioen AW. Monocyte/ macrophage infiltration in tumors: modulators of angiogenesis. J. Leukoc. Biol. 2006; 80(6):1183–1196. [PubMed: 16997855]

13. Murdoch C, Giannoudis A, Lewis CE. Mechanisms regulating the recruitment of macrophages into hypoxic areas of tumors and other ischemic tissues. Blood. 2004; 104(8):2224–2234. [PubMed: 15231578]

14. Leek RD, Lewis CE, Whitehouse R, Greenall M, Clarke J, Harris AL. Association of macrophage infiltration with angiogenesis and prognosis in invasive breast carcinoma. Cancer Res. 1996; 56(20):4625–4629. [PubMed: 8840975]

15. Hanada T, Nakagawa M, Emoto A, Nomura T, Nasu N, Nomura Y. Prognostic value of tumor-associated macrophage count in human bladder cancer. Int. J. Urol. 2000; 7(7):263–269. [PubMed: 10910229]

16. Zeisberger SM, Odermatt B, Marty C, Zehnder-Fjallman AH, Ballmer-Hofer K, Schwendener RA. Clodronate-liposome-mediated depletion of tumour-associated macrophages: a new and highly effective antiangiogenic therapy approach. Br. J. Cancer. 2006; 95(3):272–281. [PubMed: 16832418]

17. Gazzaniga S, Bravo AI, Guglielmotti A, van Rooijen N, Maschi F, Vecchi A, Mantovani A, Mordoh J, Wainstok R. Targeting tumor-associated macrophages and inhibition of MCP-1 reduce angiogenesis and tumor growth in a human melanoma xenograft. J. Invest. Dermatol. 2007; 127(8):2031–2041. [PubMed: 17460736]

18. Valable S, Barbier EL, Bernaudin M, Roussel S, Segebarth C, Petit E, Remy C. In vivo MRI tracking of exogenous monocytes/macrophages targeting brain tumors in a rat model of glioma. Neuroimage. 2007; 37(Suppl 1):S47–S58. [PubMed: 17611126]

19. Zelivyanskaya ML, Nelson JA, Poluektova L, Uberti M, Mellon M, Gendelman HE, Boska MD. Tracking superparamagnetic iron oxide labeled monocytes in brain by high-field magnetic resonance imaging. J. Neurosci. Res. 2003; 73(3):284–295. [PubMed: 12868062]

20. Engberink RD, Blezer EL, Hoff EI, van der Pol SM, van der Toorn A, Dijkhuizen RM, de Vries HE. MRI of monocyte infiltration in an animal model of neuroinflammation using SPIO-labeled monocytes or free USPIO. J. Cereb. Blood Flow Metab. 2008; 28(4):841–851. [PubMed: 18000513]

21. Moore A, Marecos E, Bogdanov A Jr, Weissleder R. Tumoral distribution of long-circulating dextran-coated iron oxide nanoparticles in a rodent model. Radiology. 2000; 214(2):568–574. [PubMed: 10671613]

22. Williams JB, Ye Q, Hitchens TK, Kaufman CL, Ho C. MRI detection of macrophages labeled using micrometer-sized iron oxide particles. J. Magn. Reson. Imaging. 2007; 25(6):1210–1218. [PubMed: 17520727]

23. Oweida AJ, Dunn EA, Karlik SJ, Dekaban GA, Foster PJ. Iron-oxide labeling of hematogenous macrophages in a model of experimental autoimmune encephalomyelitis and the contribution to signal loss in fast imaging employing steady state acquisition (FIESTA) images. J. Magn. Reson. Imaging. 2007; 26(1):144–151. [PubMed: 17659552]

24. Yancy AD, Olzinski AR, Hu TC, Lenhard SC, Aravindhan K, Gruver SM, Jacobs PM, Willette RN, Jucker BM. Differential uptake of ferumoxtran-10 and ferumoxytol, ultrasmall superparamagnetic iron oxide contrast agents in rabbit: critical determinants of atherosclerotic plaque labeling. J. Magn. Reson. Imaging. 2005; 21(4):432–442. [PubMed: 15779033]

25. Wu YL, Ye Q, Foley LM, Hitchens TK, Sato K, Williams JB, Ho C. In situ labeling of immune cells with iron oxide particles: an approach to detect organ rejection by cellular MRI. Proc. Natl. Acad. Sci. USA. 2006; 103(6):1852–1857. [PubMed: 16443687]

26. Floris S, Blezer EL, Schreibelt G, Dopp E, van der Pol SM, Schadee-Eestermans IL, Nicolay K, Dijkstra CD, de Vries HE. Blood–brain barrier permeability and monocyte infiltration in experimental allergic encephalomyelitis: a quantitative MRI study. Brain. 2004; 127(Pt 3):616–627. [PubMed: 14691063]

27. Rausch M, Sauter A, Frohlich J, Neubacher U, Radu EW, Rudin M. Dynamic patterns of USPIO enhancement can be observed in macrophages after ischemic brain damage. Magn. Reson. Med. 2001; 46(5):1018–1022. [PubMed: 11675656]

28. Sathy BN, Chou YH, Li HJ, Chang C, Chow KP. Dynamic contrast-enhanced and T2-weighted magnetic resonance imaging study of the correlation between tumour angiogenesis and growth kinetics. Lab. Anim. 2009; 43(1):53–59. [PubMed: 19015174]

29. Chow KP, Wu CC, Chang HY, Chang C, Chang YS. A simplified tumour model established via Epstein–Barr virus-encoded, nasopharyngeal carcinoma-derived oncogene latent membrane protein 1 in immunocompetent mice. Lab. Anim. 2008; 42(2):193–203. [PubMed: 18435877]

30. Ramprasad MP, Terpstra V, Kondratenko N, Quehenberger O, Steinberg D. Cell surface expression of mouse macrosialin and human CD68 and their role as macrophage receptors for oxidized low density lipoprotein. Proc. Natl. Acad. Sci. USA. 1996; 93(25):14833–14838. [PubMed: 8962141]

31. Beresford MJ, Harris AL, Ah-See M, Daley F, Padhani AR, Makris A. The relationship of the neo-angiogenic marker, endoglin, with response to neoadjuvant chemotherapy in breast cancer. Br. J. Cancer. 2006; 95(12):1683–1688. [PubMed: 17160082]

32. Qayum N, Muschel RJ, Im JH, Balathasan L, Koch CJ, Patel S, McKenna WG, Bernhard EJ. Tumor vascular changes mediated by inhibition of oncogenic signaling. Cancer Res. 2009; 69(15): 6347–6354. [PubMed: 19622766]

33. Himmelreich U, Weber R, Ramos-Cabrer P, Wegener S, Kandal K, Shapiro EM, Koretsky AP, Hoehn M. Improved stem cell MR detectability in animal models by modification of the inhalation gas. Mol. Imaging. 2005; 4(2):104–109. [PubMed: 16105508]

34. Stroh A, Zimmer C, Werner N, Gertz K, Weir K, Kronenberg G, Steinbrink J, Mueller S, Sieland K, Dirnagl U, Nickenig G, Endres M. Tracking of systemically administered mononuclear cells in the ischemic brain by high-field magnetic resonance imaging. Neuro-Image. 2006; 33(3):886–897. [PubMed: 16973381]

35. Weissleder R, Stark DD, Engelstad BL, Bacon BR, Compton CC, White DL, Jacobs P, Lewis J. Superparamagnetic iron oxide: pharmacokinetics and toxicity. Am. J. Roentgenol. 1989; 152(1): 167–173. [PubMed: 2783272]

36. Arbab AS, Wilson LB, Ashari P, Jordan EK, Lewis BK, Frank JA. A model of lysosomal metabolism of dextran coated superparamagnetic iron oxide (SPIO) nanoparticles: implications for cellular magnetic resonance imaging. NMR Biomed. 2005; 18(6):383–389. [PubMed: 16013087]

37. Vande, Berg BC.; Lecouvet, FE.; Kanku, JP.; Jamart, J.; Van Beers, BE.; Maldague, B.; Malghem, J. Ferumoxides-enhanced quantitative magnetic resonance imaging of the normal and abnormal bone marrow: preliminary assessment. J. Magn. Reson. Imaging. 1999; 9(2):322–328. [PubMed: 10077032]

38. Henning EC, Ruetzler CA, Gaudinski MR, Hu TC, Latour LL, Hallenbeck JM, Warach S. Feridex preloading permits tracking of CNS-resident macrophages after transient middle cerebral artery occlusion. J. Cereb. Blood Flow Metab. 2009; 29(7):1229–1239. [PubMed: 19417758]

39. Xu S, Jordan EK, Brocke S, Bulte JW, Quigley L, Tresser N, Ostuni JL, Yang Y, McFarland HF, Frank JA. Study of relapsing remitting experimental allergic encephalomyelitis SJL mouse model using MION-46L enhanced in vivo MRI: early histopathological correlation. J. Neurosci. Res. 1998; 52(5):549–558. [PubMed: 9632311]

40. Carmeliet P, Jain RK. Angiogenesis in cancer and other diseases. Nature. 2000; 407(6801):249–257. [PubMed: 11001068]

41. Naumov GN, Akslen LA, Folkman J. Role of angiogenesis in human tumor dormancy: animal models of the angiogenic switch. Cell Cycle. 2006; 5(16):1779–1787. [PubMed: 16931911]

42. Bergers G, Benjamin LE. Tumorigenesis and the angiogenic switch. Nat. Rev. Cancer. 2003; 3(6): 401–410. [PubMed: 12778130]

43. Lin EY, Pollard JW. Tumor-associated macrophages press the angiogenic switch in breast cancer. Cancer Res. 2007; 67(11):5064–5066. [PubMed: 17545580]

44. Lewis CE, Pollard JW. Distinct role of macrophages in different tumor microenvironments. Cancer Res. 2006; 66(2):605–612. [PubMed: 16423985]

45. van Hinsbergh VW, Engelse MA, Quax PH. Pericellular proteases in angiogenesis and vasculogenesis. Arterioscler. Thromb. Vasc. Biol. 2006; 26(4):716–728. [PubMed: 16469948]

46. Rehman J, Li J, Orschell CM, March KL. Peripheral blood 'endothelial progenitor cells' are derived from monocyte/macrophages and secrete angiogenic growth factors. Circulation. 2003; 107(8):1164–1169. [PubMed: 12615796]

47. Fernandez Pujol B, Lucibello FC, Gehling UM, Lindemann K, Weidner N, Zuzarte ML, Adamkiewicz J, Elsasser HP, Muller R, Havemann K. Endothelial-like cells derived from human CD14 positive monocytes. Differentiation. 2000; 65(5):287–300. [PubMed: 10929208]

48. De Palma M, Venneri MA, Galli R, Sergi L, Politi LS, Sampaolesi M, Naldini L. Tie2 identifies a hematopoietic lineage of proangiogenic monocytes required for tumor vessel formation and a mesenchymal population of pericyte progenitors. Cancer Cell. 2005; 8(3):211–226. [PubMed: 16169466]
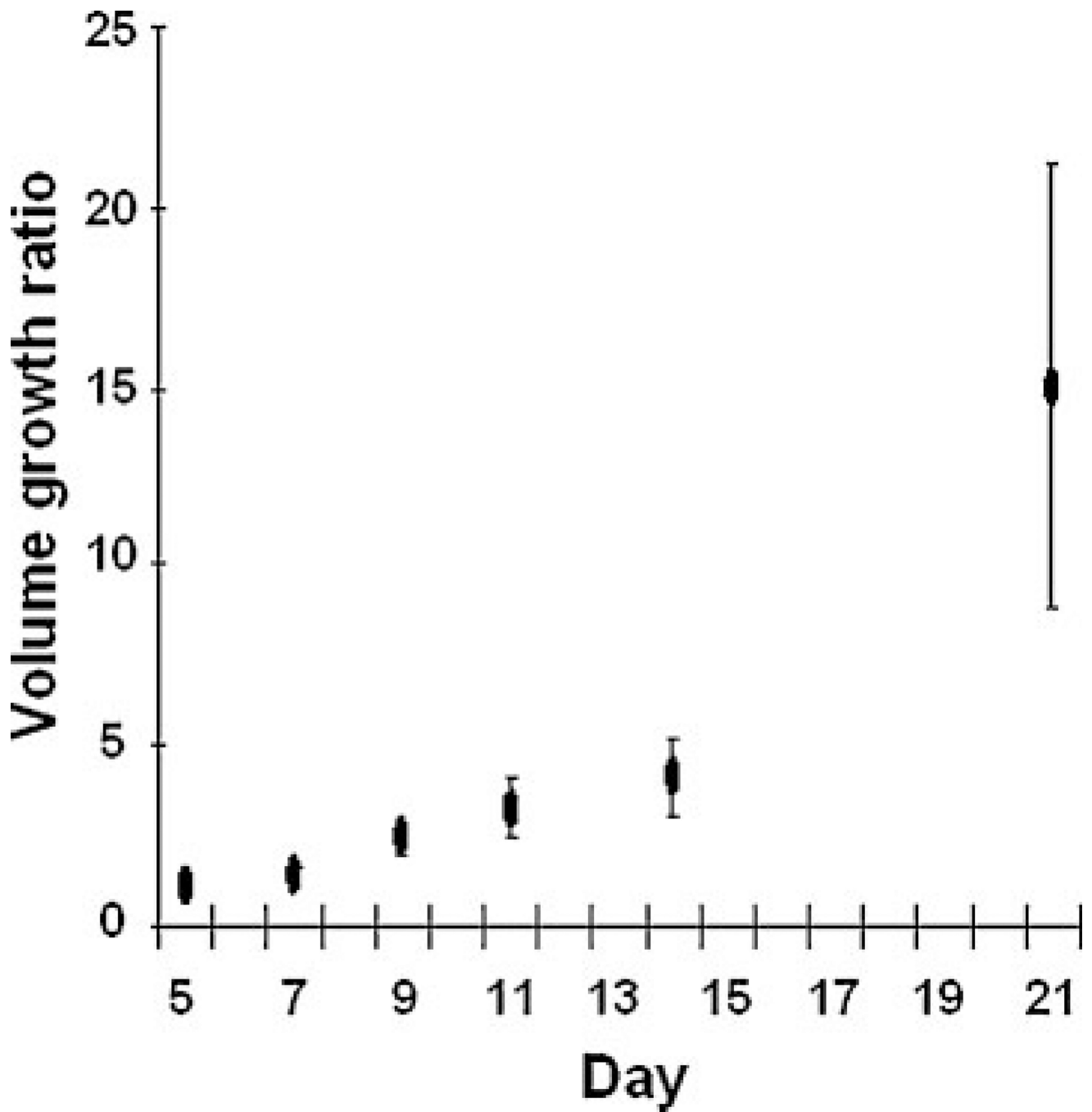
Figure 1.
Exponential growth of implanted tumor fragments. Tumor growth was defined as the volume growth ratio calculated by dividing the tumor volume at each time point by the tumor volume on day 5 ($n = 6$). The tumor growth started slowly, but increased rapidly after day 14. Error bars, standard deviation.
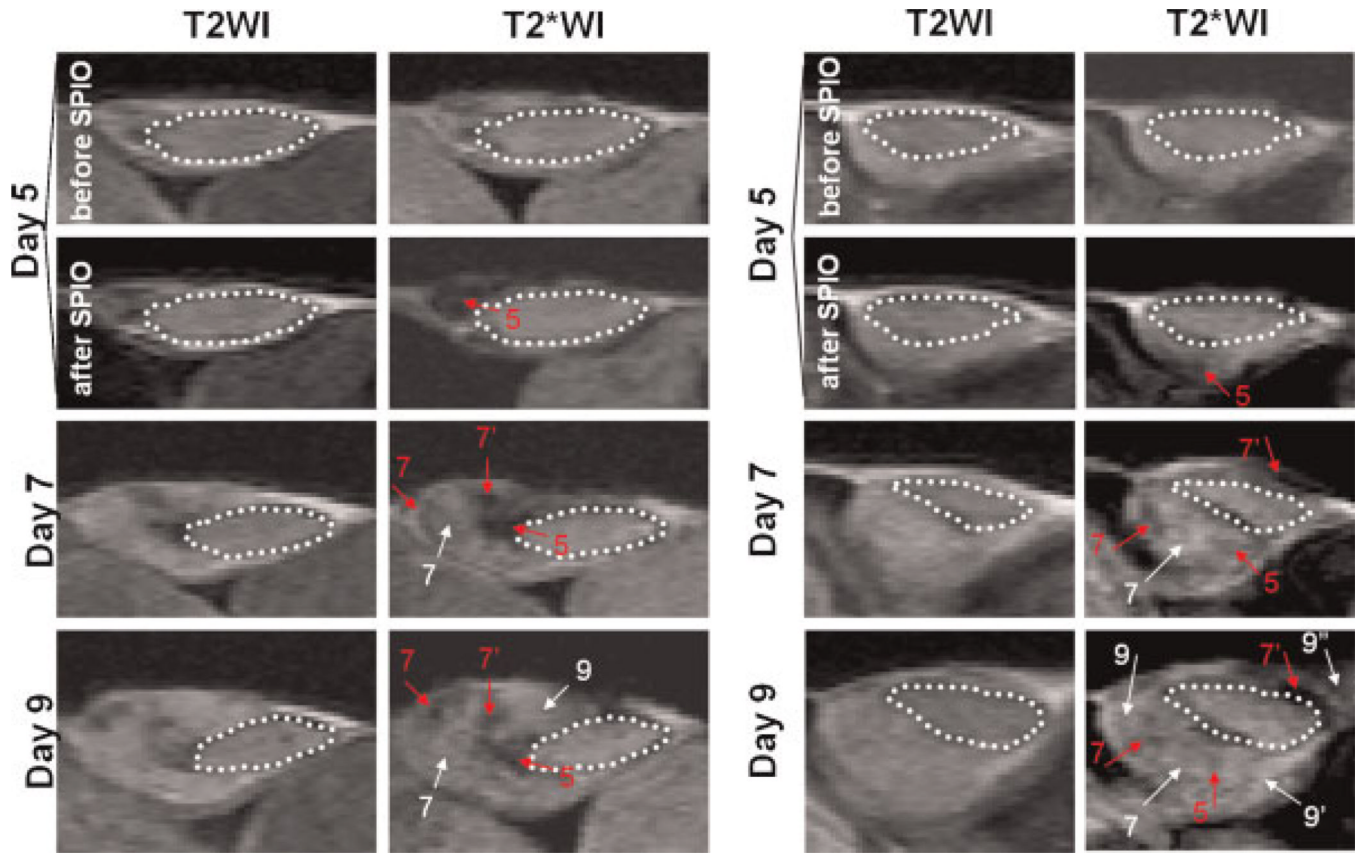
Figure 2.
MR signal loss in the growing tumor mass after injection of superparamagnetic iron oxide (SPIO) particles. The transplantable tumor model was induced by subcutaneous implantation of a solid tumor fragment (dotted circle) into the flanks of mice on day 0. Pure oxygen was delivered to the animals during imaging to enhance the MR signals in the vessels. The images are of two representative animals from a group of tumor-bearing mice shown up to day 9 ($n = 6$). On day 5, T_2- and T_2*-weighted images (T2WI and T2*WI) were acquired before and immediately after the intravenous injection of SPIO particles. MRI scanning was performed on the same animals on days 7, 9,11,14 and 21. Spots of hypointensity were assumed to be deposits of SPIO particles, whereas the hyperintensity expanding from the implanted fragment was considered to be the generation of a new tumor mass. Red and white arrows indicate the locations of hypointensities and newly generated tumor masses, respectively. The numbers with apostrophes indicate the day on which a particular spot of hypointensity/new tumor mass was first detected.
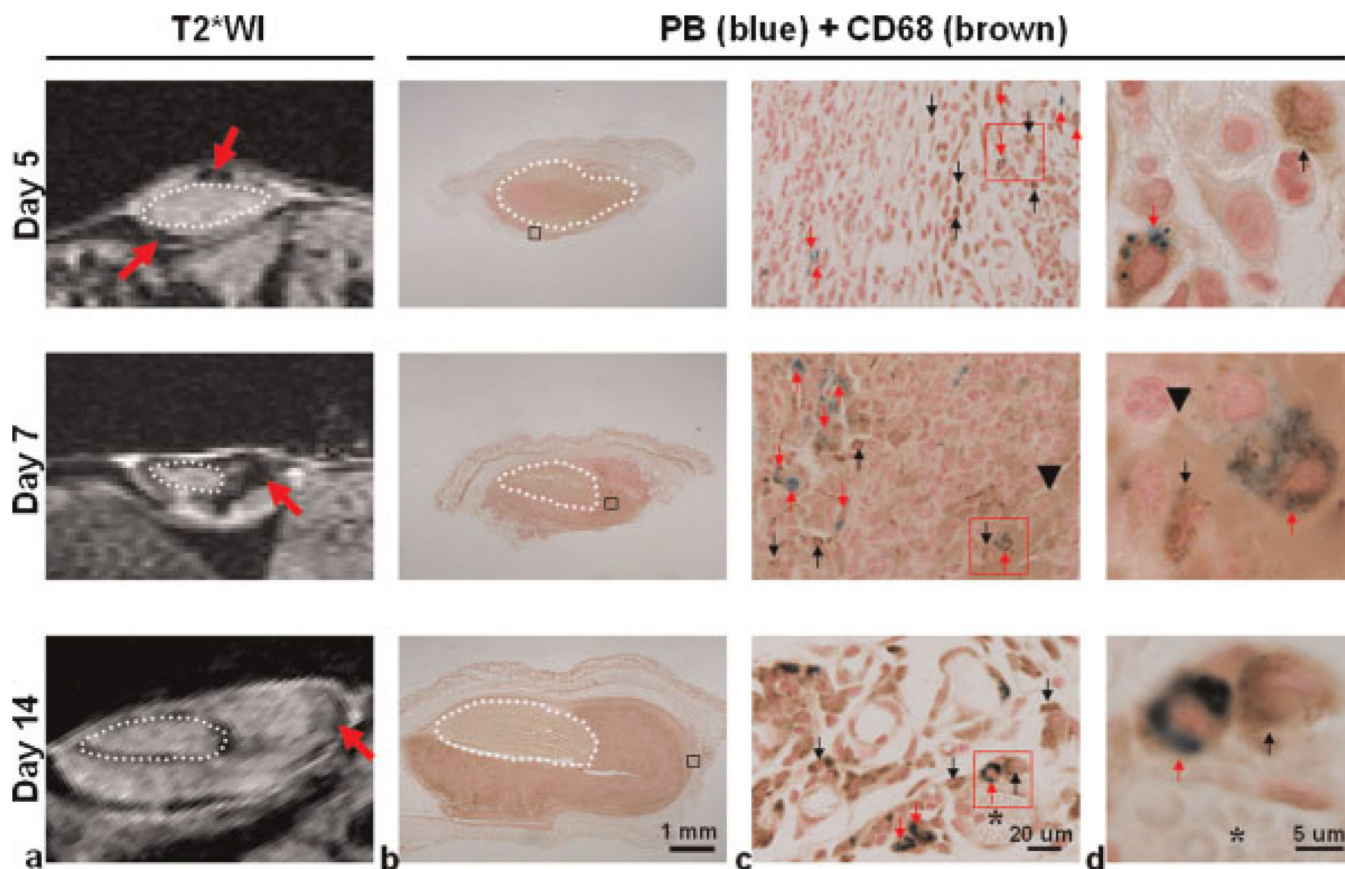
Figure 3.
Hypointensities in MR images were correlated with iron-labeled CD68-positive tumor-associated macrophages (TAMs). MRI was performed on another group of mice on days 5, 7 and 14 after injection of superparamagnetic iron oxide (SPIO) nanoparticles (total $n = 9$, $n = 3$ for each time point). After scanning, animals were sacrificed to remove the tumors, which were sectioned according to where the images were acquired. (a) T_2*-weighted images (T2*WI) show hypointensities (red arrows) in tumor tissue after SPIO injection. (b) Co-staining of Prussian blue (PB) and antibody against CD68 was used to identify the location of iron particles and CD68-positive TAMs in tumor tissue. (c) Enlarged views of the regions indicated by black squares in (b), showing the co-localization of the blue iron deposits (red arrows) and the hypointensities on the images. PB-positive and CD68-negative cells were not frequently observed. (d) Enlarged views of the regions indicated by red squares in (c), showing the cell-like structure containing blue iron particles (red arrows) and CD68 positivity in the growing tumor. PB and CD68 positivity were strongly co-localized regardless of the tumor stage, although many CD68-positive cells were located in areas without a PB reaction. Dotted circle, implanted tumor fragment; black arrowhead, hemorrhage; asterisk, vessel-like structure; red arrow, CD68-positive TAMs co-localized with PB positivity; black arrow, CD68-positive TAMs not co-localized with PB positivity.
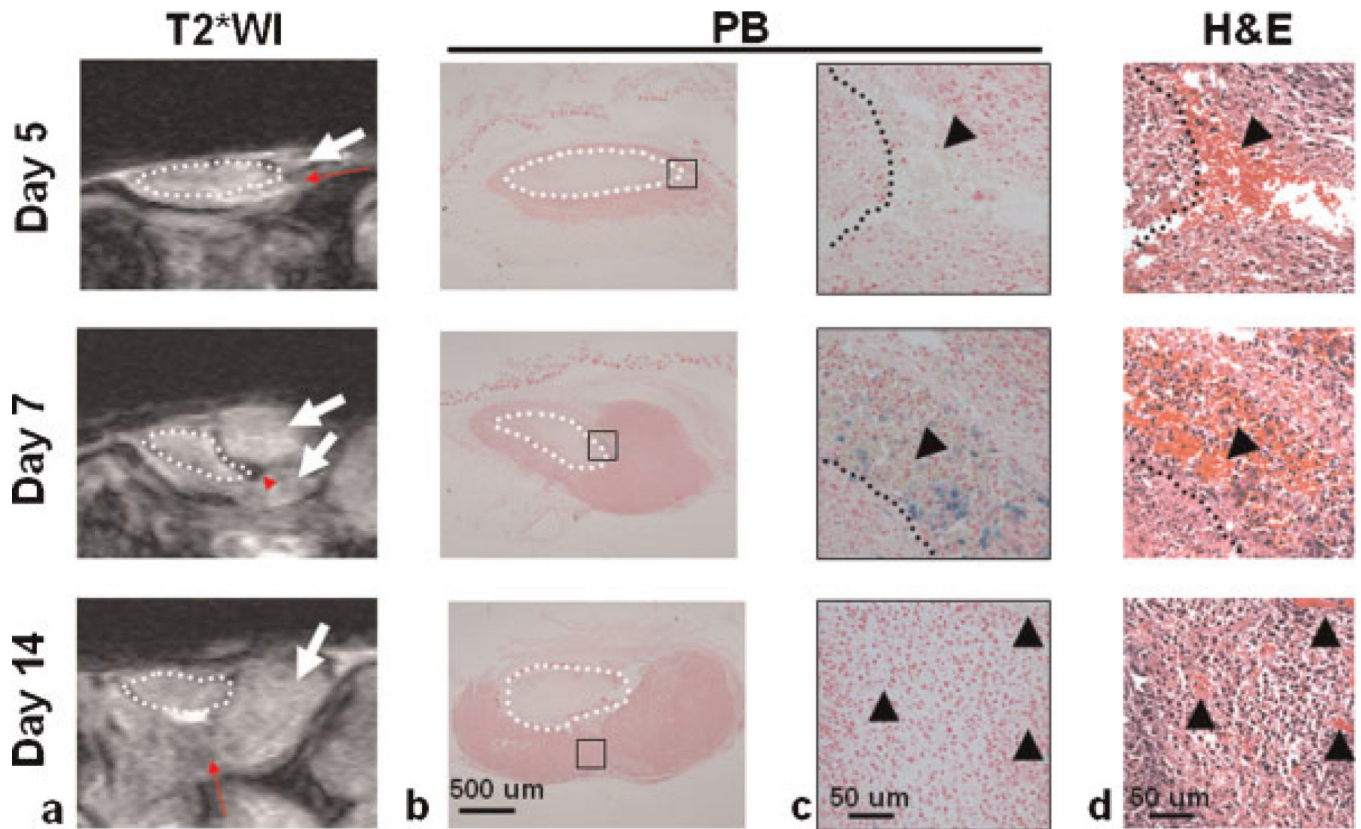
Figure 4.
Hypointensities in MR images without superparamagnetic iron oxide (SPIO) nanoparticle injection. MRI was performed on another group of mice on days 5,7 and 14 without SPIO nanoparticle injection (total $n = 6$, $n = 2$ for each time point). After scanning, animals were sacrificed to remove the tumors, which were sectioned according to where the images were acquired. (a) In T_2^*-weighted images (T2*WI), mild signal loss (red arrows) was found in the new tumor mass (white arrows) on days 5 and 14, whereas stronger hypointensity (red arrowhead) was detected on day 7. (b) Prussian blue (PB) staining was used to identify the source of MRI signal changes in the tumor tissue. (c) Enlarged views of the regions indicated by black squares in (b), demonstrating the co-localization of the blue iron deposits and the dense hypointensity on the tumor image on day 7. No blue iron deposit was observed on days 5 and 14. (d) Enlarged views of adjacent hematoxylin and eosin-stained sections (H&E), showing the co-localization of hemorrhage (black arrowheads) in the corresponding area.
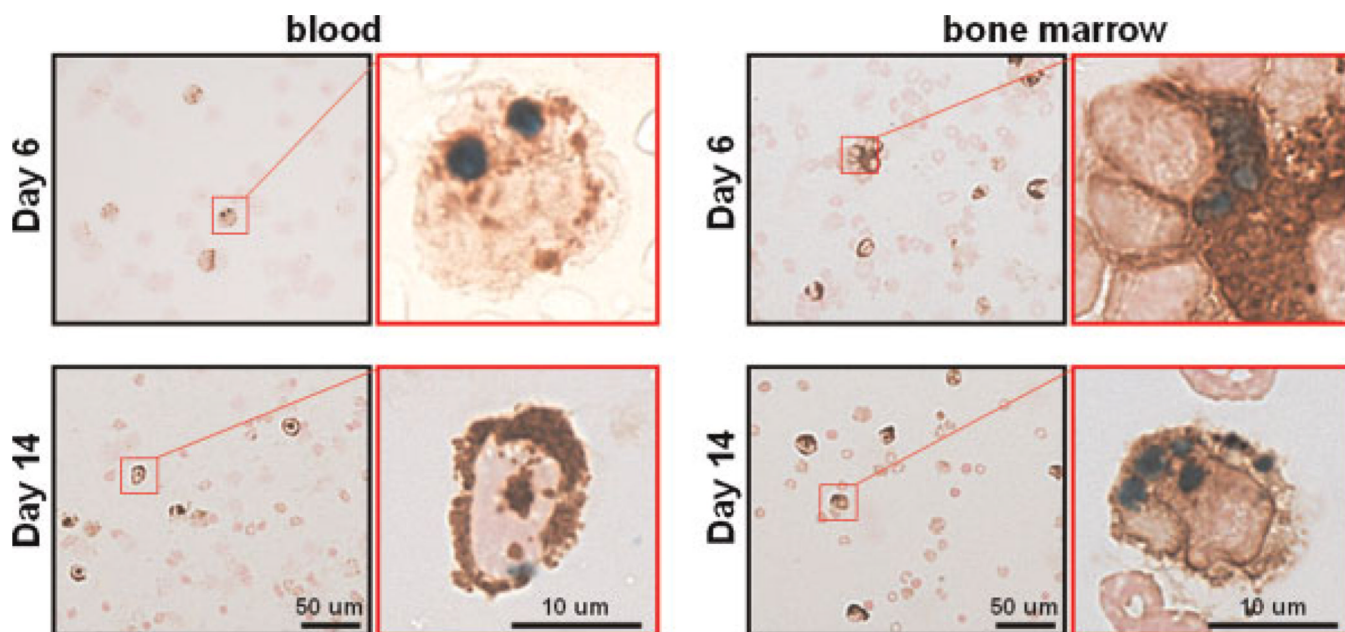
Figure 5.
The existence of superparamagnetic iron oxide (SPIO)-labeled monocytes/macrophages in blood and bone marrow. Tumor-bearing mice on days 6 and 14 after SPIO nanoparticle injection were sacrificed to extract blood and bone marrow cells ($n = 2$). The extracted cells were then co-stained with Prussian blue (PB) to detect SPIO (blue) and anti-CD68 antibody to assess monocytes/macrophages (brown). The photographs with a black frame show the existence of SPIO-labeled CD68-positive cells in the extracts, whereas the enlarged photographs with the red frame confirm the internalization of SPIO particles in the cytoplasm.
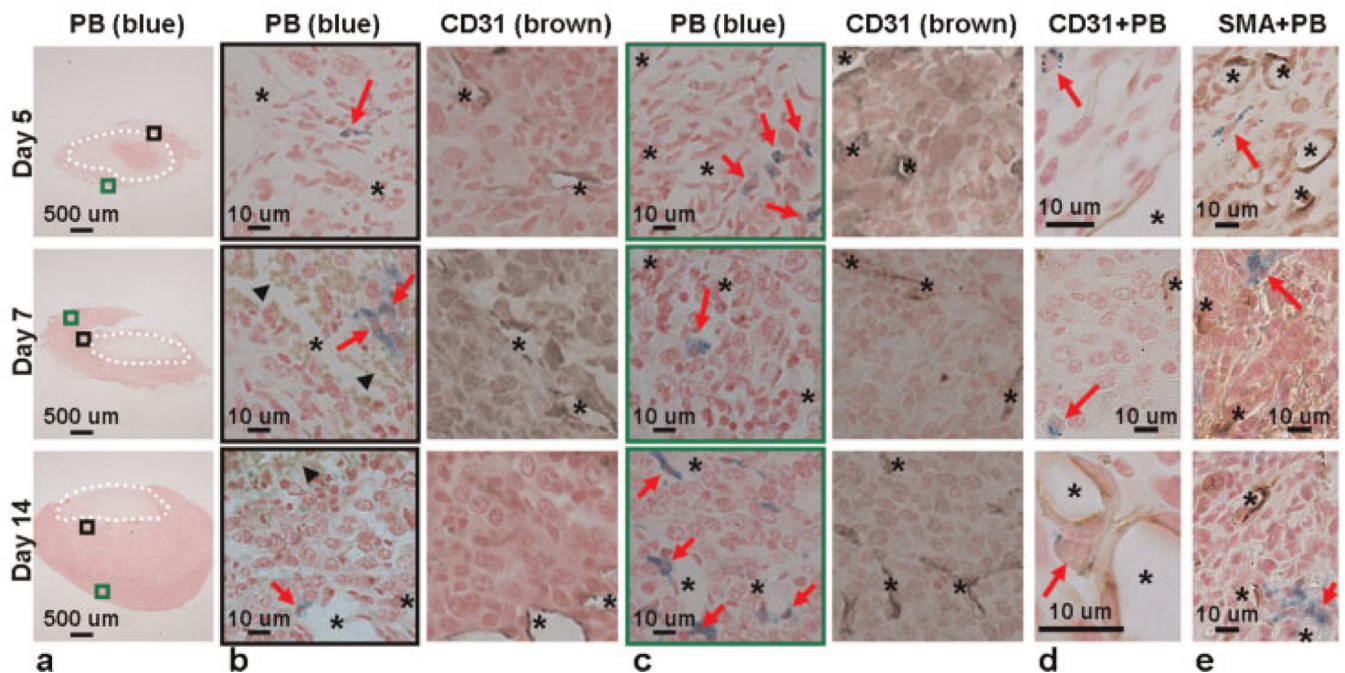
Figure 6.
Distribution preferences of superparamagnetic iron oxide (SPIO)-labeled tumor-associated macrophages (TAMs) during tumor angiogenesis. (a) Sections from collected tumors ($n = 3$ for each time point) were stained with Prussian blue (PB). (b) Enlarged views of the regions close to the tumor fragments [black squares in (a)] and the adjacent sections stained with antibody against CD31. (c) Enlarged views of the regions away from the tumor fragments [green squares in (a)] and the adjacent sections stained with antibody against CD31. PB-positive cells appeared closer to CD31-positive vessels at day 14. (d) Sections co-stained with PB and CD31. (e) Sections co-stained with PB and anti-α-smooth muscle actin (SMA) antibody. The CD31-positive endothelial cells and SMA-positive pericytes in the vessel structures contained no PB positivity, indicating that SPIO particles were not internalized by epithelial cells and/or pericytes/myofibroblasts in the vessel wall. Dotted circle, implanted tumor fragment; red arrow, SPIO-labeled cell; black arrowhead, hemorrhage; asterisk, CD31- or SMA-positive vessel.